New Polymeric Manganese Azide Derivatives with Quinazoline

Morsy A. M. Abu-Youssef,*[a] Albert Escuer,[b] and Vratislav Langer[c]

Keywords: Azides / Coordination polymers / Magnetic properties / Manganese

Two new polymeric derivatives of the (azido)Mn^{II} system with formula $[Mn(H_2O)(\mu\text{-}N_3)(N_3)(quinaz)_2]_n$ (**1**) and $[Mn(\mu\text{-}N_3)_2(quinaz)_2]_n$ (**2**) (quinaz = quinazoline) have been structurally and magnetically characterised. Compound **1** crystallises in the triclinic system, space group $P\bar{1}$, and consists of 1D chains with single end-to-end azido bridges. These chains give a two-dimensional supramolecular arrangement by means of H-bond interactions. Compound **2** crystallises in the monoclinic system, space group $C2/c$, and contains a square alternating 2D network bridged by azido ligands in the end-to-end coordination mode. Compound **2** exhibits some unusual features, such as the unprecedented linear coordination of the azido bridge. Magnetic analysis reveals moderate antiferromagnetic coupling, with J values in good agreement with the expected range, as a function of the Mn–N–N bond angles.

Introduction

The azido ligand is currently one of the most interesting bridging ligands in the attempt to build polynuclear or *n*-dimensional architectures, which combine its interest as a ligand in coordination chemistry with a large variety of magnetic responses.[1] The versatility of this ligand is a direct consequence of its ability to act as a bridge in a large variety of coordination modes. For example, it is able to link two cations [in either end-to-end (EE)[2–4] or end-on (EO)[3,5] modes], three cations in the more exotic $\mu_{1,1,1}$ or $\mu_{1,1,3}$ modes,[4] or act as a bridge between four metallic centres in the rare examples of $\mu_{1,1,1,1}$ and $\mu_{1,1,3,3}$ modes.[5] The simultaneous presence of more than one of these coordination modes in the same compound is not rare, and this increases the number of possible topologies.[6,7] The interest of magnetochemists in this ligand lies in the well-established relationship between its coordination mode and the resulting magnetic properties, which cover a wide range of ferro-, ferri- and antiferromagnetic responses,[1] although it should be pointed out that the topology of the resulting systems is far from being controllable. The large structural variations of azide derivatives reported in the last few years provides experimental proof of the effects of minor changes in the synthetic conditions or in the co-ligands bridged to the metallic centre. One of the most complete series of compounds, with general formula $[Mn(N_3)_2(R\text{-}py)_2]_n$, (R-py = substituted pyridyl ligands) is a paradigmatic example of how minor differences in R can change the dimensionality or the coordination mode of the azido bridges, which are generally related to weak supramolecular π–π stacking interactions or to the packing forces in the solid, drastically.

In this paper, we present the synthesis and X-ray and magnetic characterisation of two new polymeric manganese azide derivatives with formula $[Mn(H_2O)(\mu\text{-}N_3)(N_3)(quinaz)_2]_n$ (**1**) and $[Mn(\mu\text{-}N_3)_2(quinaz)_2]_n$ (**2**). The co-ligand quinazoline (quinaz) was chosen in order to combine the versatility of the azido ligand with the possibility of a second bridging ligand closely related to previously reported systems such as pyrimidine,[8] but introducing structural differences in the ligand in order to generate new topologies. The resulting compounds show that quinaz, in contrast to pyrimidine, coordinates through only one of its donor N-atoms in a similar way to classical pyridine ligands. Compound **1** is a 1D alternating system with single EE bridges in a *cis* arrangement, giving an uncommon 1D zigzag topology. Extended H-bonds between terminal azide and water molecules coordinated to the manganese atom generate a supramolecular 2D network. Compound **2** is an alternating square 2D layer of manganese EE azido bridges with *trans*-quinaz coordinated ligands. The magnetic behaviour agrees with the antiferromagnetic coupling expected for this kind of bridge.

[a] Chemistry Department, Faculty of Science, Alexandria University,
P. O. Box 426, Ibrahimia, 21321 Alexandria, Egypt
Fax: +20-3-391-1794
E-mail: morsy5@link.net
[b] Departament de Química Inorgànica, Universitat de Barcelona, Martí I Franqués 1-11, 08028-Barcelona, Spain
Fax: +34-93-490-7725
E-mail: albert.escuer@qi.ub.es
[c] Department of Chemical and Biological Engineering, Division of Materials and Surface Chemistry, Subdivision of Environmental Inorganic Chemistry, Chalmers University of Technology,
41296 Göteborg, Sweden
Fax: +46-31-772-2853
E-mail: langer@chalmers.se

Results and Discussion

Synthesis

Slow concentration of water/methanol solutions of manganese nitrate tetrahydrate, the quinazoline ligand and sodium azide gave single crystals of **1** (cold solutions) and **2** (room temperature crystallization).

Structure of $[Mn(H_2O)(\mu\text{-}N_3)(N_3)(quinaz)_2]_n$ (1)

A labelled ORTEP plot of the structure is shown in Figure 1. Selected distances and angles are listed in Table 1. The structure of this compound can be described as zigzag chains of manganese atoms linked by single azido bridges coordinated in the EE mode.

The manganese atoms are placed in an octahedral environment and are linked to two quinazoline ligands in a *trans* position, two azide N atoms corresponding to the bridging end-to-end ligands, one terminal azido and one water molecule. Larger bond lengths are found to the N(quinazoline) atoms (2.318 Å), intermediate distances (around 2.2 Å) to the N(azide) atoms and a shorter distance (2.179 Å) to the O atom. The azido bridges along the chain are not equivalent and show similar, but not identical, Mn–N–N bond angles [142.6° for Mn(1)–N(11)–N(12) and 137.3° for Mn(1)–N(31)–N(32)]. The terminal azido ligand shows a larger Mn(1)–N(21)–N(22) bond angle of 150.4°. The torsion angle for the two non-equivalent Mn–N–N–N–Mn units is 180°. The water molecule and the N(23) atom

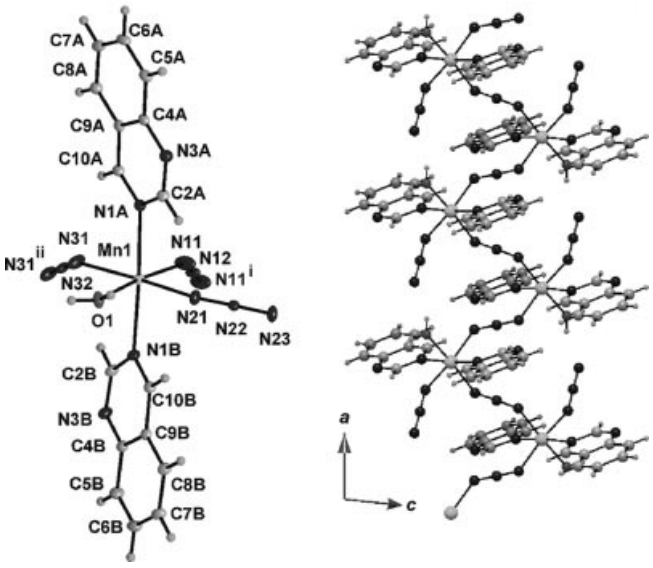

Figure 1. Left: labelled ORTEP plot of the basic unit of $[Mn(H_2O)(\mu\text{-}N_3)(N_3)(quinaz)_2]_n$ (**1**) with thermal ellipsoids at 30% probability. Right: 1D structure shown in projection along the *b*-axis.

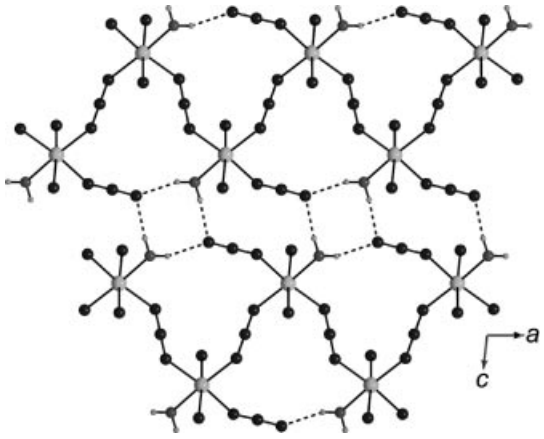

Figure 2. View of the zigzag arrangement of the individual chains of $[Mn(H_2O)(\mu\text{-}N_3)(N_3)(quinaz)_2]_n$ (**1**) and the 2D arrangement generated from the interaction of H(11) and H(12) with the terminal N(23) atoms.

Table 1. Selected bond lengths [Å] and angles [°] for $[Mn(H_2O)(\mu\text{-}N_3)(N_3)(quinaz)_2]_n$ (**1**).[a]

Mn(1)–N(1A)	2.318(1)	N(11)–N(12)	1.169(1)	
Mn(1)–N(1B)	2.318(1)	N(12)–N(11)i	1.169(1)	
Mn(1)–N(11)	2.205(1)	N(21)–N(22)	1.171(1)	
Mn(1)–N(21)	2.188(1)	N(22)–N(23)	1.174(1)	
Mn(1)–N(31)	2.215(1)	N(31)–N(32)	1.175(1)	
Mn(1)–O(1)	2.179(1)	N(32)–N(31)ii	1.175 (1)	
N(1A)–Mn(1)–N(1B)	173.64(4)	Mn(1)–N(11)–N(12)	142.6(1)	
N(1A)–Mn(1)–N(11)	94.24(5)	Mn(1)–N(21)–N(22)	150.4(1)	
N(1A)–Mn(1)–N(21)	89.56(4)	Mn(1)–N(31)–N(32)	137.3(1)	
N(1A)–Mn(1)–N(31)	89.71(4)			
N(1A)-Mn(1)- O(1)	88.60(4)	N(11)–N(12)–N(11)i	180.00	
N(1B)–Mn(1)–N(11)	92.01(5)	N(21)–N(22)–N(23)	178.1(1)	
N(1B)–Mn(1)–N(21)	88.89(4)	N(31)–N(32)–N(31)ii	180.00	
N(1B)–Mn(1)–N(31)	91.09(4)			
N(1B)–Mn(1)–O(1)	85.07(4)			
N(11)–Mn(1)–N(21)	93.46(6)	H-bonds	O···N	O–H···N
N(11)–Mn(1)–N(31)	93.48(6)	O(1)–H(11)···N(23)iii	2.775(2)	159(2)
N(11)–Mn(1)–O(1)	174.02(5)	O(1)–H(12)···N(23)iv	2.829(2)	175(2)
N(21)–Mn(1)–N(31)	173.06(5)			
N(21)–Mn(1)–O(1)	81.28(4)			
N(31)–Mn(1)–O(1)	91.80(5)			

[a] Symmetry transformations used to generate equivalent atoms: (i): $-x + 2, -y + 1, -z + 1$; (ii): $-x + 1, -y + 1, -z + 1$; (iii): $x - 1, y, z$; (iv): $-x + 2, -y + 1, -z + 2$; (v): $x, y - 1, z$.

from the terminal azido ligand are related by means of H-bonds through H(11) and H(12) giving a 2D supramolecular arrangement (Figure 2). The Mn···Mn intrachain distances are 6.426(1) Å [bridge N(11)–N(12)–N(11)′] and 6.360(1) Å [bridge N(31)–N(32)–N(33)]. The minimum interchain Mn···Mn distance is 7.214(1) Å.

Structure of $[Mn(\mu\text{-}N_3)_2(quinaz)_2]_n$ (2)

A labelled ORTEP plot of the structure is shown in Figure 3. Selected distances and angles are listed in Table 2. The structure consists of a 2D square network of Mn^{II} cations bridged by EE azido bridges (Figure 4).

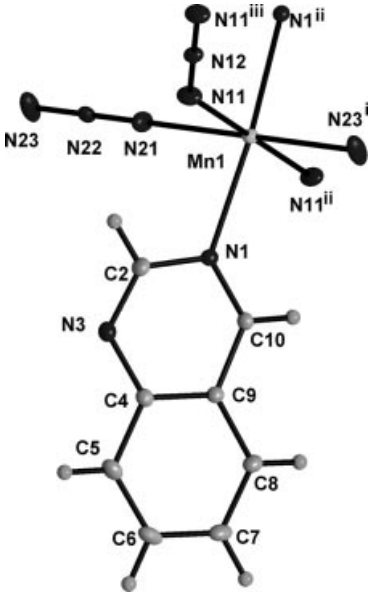

Figure 3. Labelled ORTEP plot of the basic unit of $[Mn(\mu\text{-}N_3)_2(quinaz)_2]_n$ (**2**) with thermal ellipsoids at 50% probability.

Each manganese atom is surrounded by two quinazoline ligands in a *trans* position and four N(azide) atoms, which act as a bridge to the four neighbouring manganese atoms. As observed in **1**, the Mn–N(quinazoline) bonds (ca. 2.285 Å) are longer than those found for the Mn–N(azide) bonds (2.217–2.254 Å). The Mn–N–N bond angles show large differences: Mn(1)–N(11)–N(12) is 144.3(1)°, which lies in the normal range for this ligand, whereas the two bond angles Mn(1)–N(21)–N(22) and Mn(1)iv–N(23)–N(22) have a value of 180°, which means that this Mn–NNN–Mn subunit is fully linear. The torsion angle for the Mn–N(11)–N(12)–N(13)–Mn units is 180°. The Mn···Mn intraplane distances are 6.8045(1) Å [bridge N(21)–N(22)–N(23)] and 6.4921(1) Å [bridge N(11)–N(12)–N(11)′], and the minimum interplane Mn···Mn distance is 9.845(1) Å.

The most singular detail of this structure is the linear coordination of one of the azide bridges. Some unusually large Mn–N–N bond angles have previously been found in the 2D system $[Mn(DENA)_2(N_3)_2]$ (DENA = diethylnicotinamide),[9] for which one of the bridges exhibits a pair of Mn–N–N bond angles of 148.4° and 171.7°. Large bond angles have also been found in one dinuclear (cryptand)

Table 2. Selected bond lengths [Å] and angles [°] for $[Mn(\mu\text{-}N_3)_2(quinaz)_2]_n$ (**2**).[a]

Mn(1)–N(1)	2.285(1)	N(11)–N(12)	1.171(1)
Mn(1)–N(1)ii	2.285(1)	N(12)–N(11)iii	1.171(1)
Mn(1)–N(11)	2.222(1)	N(21)–N(22)	1.158(3)
Mn(1)–N(11)ii	2.222(1)	N(22)–N(23)	1.175(3)
Mn(1)–N(21)	2.254(2)		
Mn(1)–N(23)i	2.217(2)		
N(1)–Mn(1)–N(1)ii	174.68(6)	Mn(1)–N(11)–N(12)	144.3(1)
N(1)–Mn(1)–N(11)	88.41(5)	Mn(1)–N(21)–N(22)	180.0
N(1)–Mn(1)–N(11)ii	91.60(5)	Mn(1)iv–N(23)–N(22)	180.0
N(1)–Mn(1)–N(21)	87.34(3)		
N(1)–Mn(1)–N(23)i	92.66(3)		
N(1)ii–Mn(1)–N(11)	91.60(5)	N(11)–N(12)–N(11)iii	180.0
N(1)ii–Mn(1)–N(11)ii	88.41(5)	N(21)–N(22)–N(23)	180.00(1)
N(1)ii–Mn(1)–N(21)	87.34(3)		
N(1)ii–Mn(1)–N(23)i	92.66(3)		
N(11)–Mn(1)–N(11)ii	179.79(8)		
N(11)–Mn(1)–N(21)	90.10(4)		
N(11)–Mn(1)–N(23)i	89.90(4)		
N(11)ii–Mn(1)–N(21)	90.10(4)		
N(11)ii–Mn(1)–N(23)i	89.90(4)		
N(21)–Mn(1)–N(23)i	180.0		

[a] Symmetry transformations used to generate equivalent atoms: (i): $x, y-1, z$; (ii): $-x, y, -z+1/2$; (iii): $-x, -y, -z$; (iv): $x, y+1, z$; (v): $x, -y, z+1/2$.

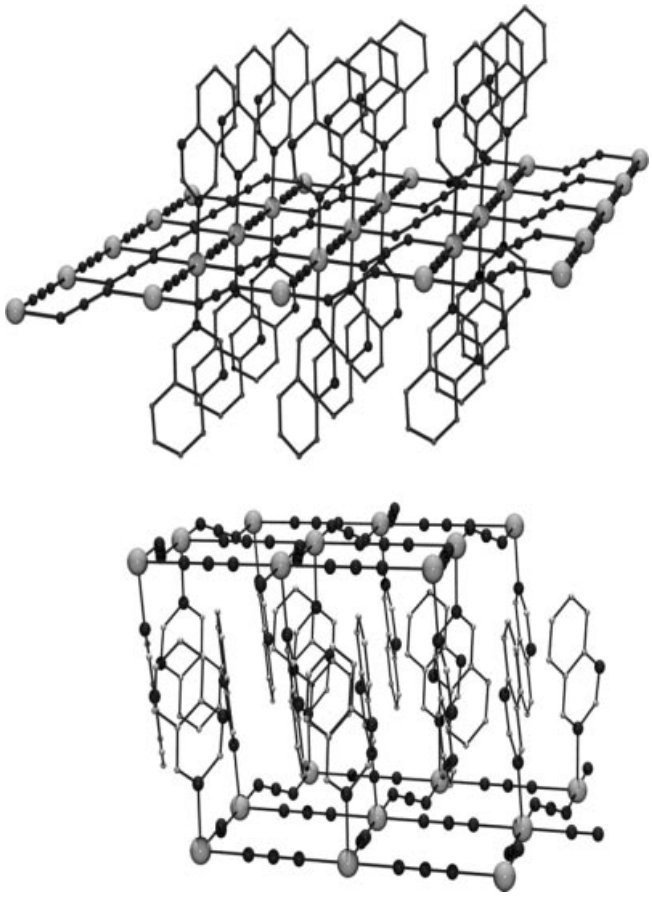

Figure 4. Top: view of one layer of $[Mn(\mu\text{-}N_3)_2(quinaz)_2]_n$ (**2**). In this figure the linear manganese–azido bonds along the *b*-axis can be clearly differentiated. Bottom: view of the interlayer π–π stacking between adjacent sheets.

Mn^{II} compound,[10] but in all cases the coordination of the bridge is far from linear.

Magnetic Measurements and Coupling Constant Calculations

The magnetic measurements were performed on powdered crystalline samples in the 2–300 K temperature range. The overall interaction is moderately antiferromagnetic for the two compounds.

The plot of the susceptibility vs. temperature for compound **1** shows a regular increase on cooling up to a maximum value at 20 K (Figure 5). The $\chi_M T$ value at room temperature is 3.93 $cm^3 K mol^{-1}$ for the manganese atom, which is lower than the expected value for an isolated Mn^{II} ion (4.375 $cm^3 K mol^{-1}$), and decreases continuously, tending to zero at low temperature. Based on the structural data, compound **1** is strictly an alternating one-dimensional system which shows similar bond lengths, identical torsion angles and quite similar Mn–N–N bond angles in the bridging region. Two alternative and complementary fits were performed on the χ_M data in order to determine coherent values for the coupling constants. The first fit was made assuming that the differences in the bond parameters are a minor effect, and the fit of the experimental data was performed as a system with only one average J coupling constant by applying the analytical expression for a regular chain derived from the Hamiltonian $H = -JS_i \cdot S_{i+1}$ for local $S = 5/2$.[11] The best-fit parameters were $J = -4.4(1)$ cm^{-1} and $g = 2.00(1)$ (paramagnetic impurities: 1.3%). As would be expected from the similar bond parameters, attempts to differentiate two J coupling constants in a second fit on the basis of the Hamiltonian $H = J_1 \Sigma S_{2i} \cdot S_{2i+1} - J_2 \Sigma S_{2i+1} \cdot S_{2i+2}$, as proposed by Drillon et al.,[12] did not improve the results obtained in the fit as a homogeneous chain, giving similar J_1 and J_2 values around the –4.35 cm^{-1} average value.

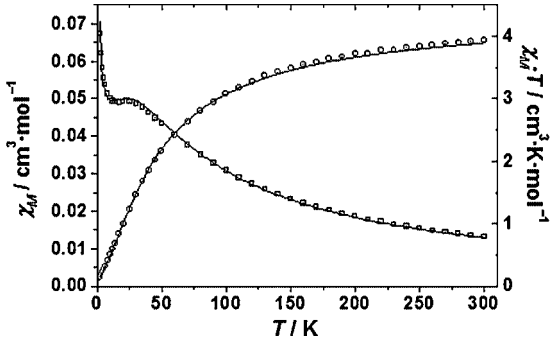

Figure 5. Plot of χ_M (open squares) and $\chi_M T$ product (open circles) for compound **1**. Solid lines correspond to the best fit (see text).

Compound **2** shows a similar shape for the susceptibility plot, with a maximum at 32 K and a $\chi_M T$ value of 4.04 at room temperature (Figure 6). In this case, the structural data indicate a 2D system with two clearly different J coupling constants, as would be expected from the very different Mn–N–N bond angles found in the network. Analytical expressions for the calculation of the coupling constants for systems of this kind are not available, so only an approximation can be made for **2**. The fit as a simplified 2D quadratic layer by means of the high-temperature expansion series derived from the Hamiltonian $H = \Sigma_{nn} - JS_iS_j$, (where Σ_{nn} runs over all pairs of nearest spins i and j),[13] gives a relatively poor fit [dotted line in Figure 6, $J = -2.5$ cm^{-1}, $g = 2.00(1)$], thus indicating that the magnetic behaviour of this system is far from a homogeneous 2D response. Not surprisingly, a better fit of the experimental data was obtained by treating the system as a homogeneous 1D system [solid line in Figure 6, $J = -4.9(1)$ cm^{-1}, $g = 2.03(1)$].

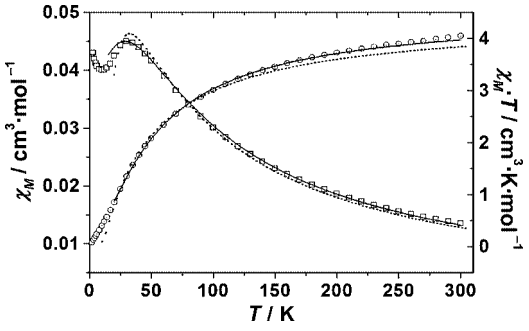

Figure 6. Plot of χ_M (open squares) and $\chi_M T$ product (open circles) for compound **2**. The dotted line shows the best fit as a homogeneous 2D system. The solid line shows the best fit as a one-dimensional system (see text).

Magnetostructural Correlations

As was calculated previously,[14] the superexchange interaction for a d^5 ion should be antiferromagnetic in nature and mediated by two kind of pathways. The main interaction goes via σ-interactions involving one of the non-bonding π-MOs of the azide and the atomic e_g-orbitals of the metallic ions. As shown in Figure 7,[14] this interaction pathway is very effective at small Mn–N–N bond angles and is practically negligible for large bond angles. The contribution of this pathway to the antiferromagnetic component of the interaction is therefore very sensitive to the experimental Mn–N–N bond angle. This fact has been checked experimentally for Cu^{II} and Ni^{II} cryptand systems with M–N–N bond angles close to 165°,[10] for which the antiferromagnetic component is close to zero and the global coupling is ferromagnetic. The second interaction pathway, which is active in our case, corresponds to pπ–dπ interactions between the non-bonding π-MOs of the azido and two of the atomic t_{2g}-orbitals of the metallic ion (Scheme 1). This second interaction mechanism is much less effective than the σ-pathway due to the worse overlap at any Mn–N–N angle value.[10]

Compound **1** is an alternating system with similar Mn–N–N bond angles. From Figure 7, is easy to justify the reason for the failure of the fit as an alternating system: the antiferromagnetic components for the two kinds of bridges should be very similar and therefore the two J values cannot be differentiated. The calculated J value as a homogeneous chain can be assumed as a good mean value with poor

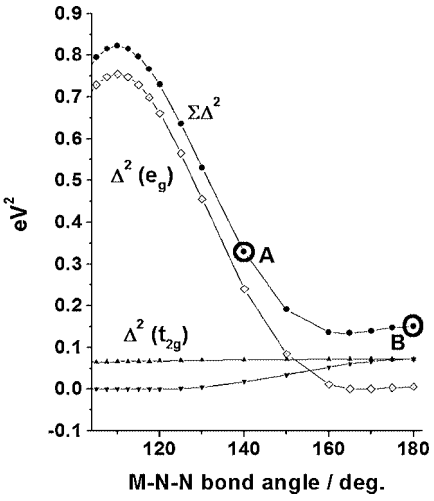

Figure 7. Walsh diagram of the Δ^2 gaps. Filled triangles correspond to the t_{2g}-components, open diamonds show the e_g-component and the filled circles show the global contribution to the antiferromagnetic interaction for a d^5-ion like Mn^{II}. Points A and B correspond to the antiferromagnetic contribution for 145° and 180° Mn–N–N bond angles, respectively.

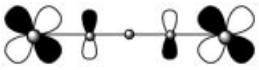

Scheme 1. One of the pπ–dπ superexchange pathways that are active for d^5-ions bridged by a linear azido bridge.

deviation for these bond parameters. Comparison with other 1D azido systems with similar bond parameters is reasonable.[1]

Compound **2** shows two very different bond angles, one of which (144.1°) is slightly larger than the mean values of compound **1**, and 180° for the second Mn–N–N bond angle. Therefore a moderate antiferromagnetic coupling should be expected for the bridge with normal bond angles for compound **2** (A in Figure 7), in contrast to the much lower antiferromagnetic coupling for the linear bridge (B in Figure 7) and agreeing with the poor fit as a 2D system with only one mean *J* value. It is obviously erroneous to assume that the interaction mediated by the linear Mn^{II}–azido units is negligible, and it is not surprising that the susceptibility plot shows better fit as a 1D system and with a calculated *J* value close to compound **1**. It is not possible to evaluate the correct *J* values from analytical fits, but the above result is indicative of the low antiferromagnetic contribution of the 180° azido bridge, as expected from theoretical predictions.[14]

Conclusions

The reported results are new examples of the importance of synthetic conditions and weak supramolecular interactions in the resulting topologies of high-dimensional manganese azide systems. Compound **2** shows an unprecedented linear coordination between two metallic centres, which has not been obtained even with previously studied cryptand systems. This kind of coordination can be assumed to be a special case of the EE coordination mode. Magnetic measurements afford the first experimental confirmation of the low antiferromagnetic coupling for such large Mn–N–N bond angles, as was predicted previously.

Experimental Section

General Remarks: Magnetic susceptibility measurements were carried out on polycrystalline samples with a Quantum Design susceptometer working in the 2–300 K range in a magnetic field of 0.3 T and remeasured in a field of 0.03 T in the 20–2 K range. Diamagnetic corrections were estimated from Pascal's tables. Infrared spectra (4000–200 cm^{-1}) were recorded from KBr pellets with a Bruker IFS-125 FT-IR spectrophotometer.

$[Mn(N_3)_2(H_2O)(quinaz)_2]_n$ (1): A solution of quinazoline (0.52 g, 4 mmol) in methanol (15 mL) was added to a methanolic solution (15 mL) of manganese nitrate tetrahydrate (0.5 g, 2 mmol). Then, a concentrated aqueous solution of sodium azide (0.65 g, 10 mmol) was added dropwise with continuous stirring. The resulting clear solution was allowed to stand for several days in a refrigerator. Yellow crystals suitable for X-ray measurements were collected and dried in air. Yield: 0.58 g (70%). $C_{16}H_{14}MnN_{10}O$ (417.31): calcd. C 46.04, H 3.35, Mn 13.16, N 33.57; found C 45.98, H 3.11, Mn 12.89, N 34.14. IR (KBr): $\tilde{\nu}$ = 3347 vs, 3233 vs, 3043 ms, 2122 vs, 2089 vs, 1619 vs, 1573 vs, 1554 w, 1519 w, 1489 vs, 1465 m, 1428 m, 1408 m, 1381 vs, 1306 s, 1277 m, 1257 m, 1239 m, 1212 vs, 1154 w, 1139 s, 1065 s, 1013 m, 987 m, 955 vs, 930 vs, 874 s, 832 s, 794 vs, 762 vs, 633 vs, 593 vs, 521 s, 473 vs, 409 wm, 387 m, 368 m, 343 m, 316 m, 293 m, 269 vs cm^{-1}.

$[Mn(N_3)_2(quinaz)_2]_n$ (2): An aqueous solution (10.0 mL) of manganese nitrate tetrahydrate (0.25 g, 1.0 mmol) was mixed with a methanolic solution (10 mL) of quinazoline (0.26 g, 2.0 mmol) and the mixture was stirred for about 5 min. A solution of sodium azide (0.32 g, 5 mmol) in water (5 mL) was then added dropwise with vigorous stirring. The resulting clear solution was allowed to stand at room temperature for several weeks. Brown-yellowish crystals suitable for X-ray measurements were collected and dried in air. Yield: 0.26 g (65%). $C_{16}H_{12}MnN_{10}$ (399.30): calcd. C 48.12, H 3.00, Mn 13.76, N 35.08; found C 47.98, H 3.11, Mn 13.89, N 35.24. IR (KBr): $\tilde{\nu}$ = 3439 w, 3046 w, 2096 vs, 1618 s, 1573 s, 1489 s, 1458 m, 1409 m, 1379 s, 1308 m, 1269 m, 1239 m, 1210 ms, 1139 ms, 1103 wm, 1066 ms, 1012 wm, 983 wm, 955 ms, 926 m, 881 m, 832 m, 795 s, 762 s, 636 s, 617 m, 598 m, 588 m, 524 wm, 479 m, 451 vw, 409 vw, 387 vw, 367 vw, 343 vw, 317 vw, 294 vw, 269 m, 235 s cm^{-1}.

It should be pointed out that the two compounds were obtained with the same stoichiometric ratio of reagents. The factors that control the final compound are difficult to evaluate and the solubility of the products, the temperature and the reaction time play an important role. In this case, the coordination of a second azido ligand in **2** in comparison with **1** is probably related to the higher temperature of the reaction mixture that favours the replacement of the coordinated water molecule.

X-ray Crystallographic Study: All diffraction data were collected with a Siemens SMART CCD diffractometer with Mo-K_α radiation (λ = 0.71073 Å, graphite monochromator). The crystals were cooled to 173(2) K by a flow of nitrogen gas using an LT-2A device. Full spheres of reciprocal lattices were scanned by 0.3° steps in ω with a crystal-to-detector distance of 3.97 cm. Preliminary orientation matrices were obtained from the first frames using SMART.

The collected frames were integrated using the preliminary orientation matrices, which were updated every 100 frames. Final cell parameters were obtained by refinement on the positions of reflections with $I > 10\sigma(I)$ after integration of all the frames with SAINT.[15] The data were empirically corrected for absorption and other effects with SADABS.[16] The structures were solved by direct methods and refined by full-matrix least squares on all F^2 data with SHELXTL.[17] The non-H atoms were refined anisotropically, while hydrogen atoms were refined isotropically with the use of geometrical restraints. Selected crystallographic and refinement data are summarised in Table 3. Molecular graphics were prepared with Diamond.[18] CCDC-264957 (**1**) and -264958 (**2**) contain the supplementary crystallographic data for this paper. These data can be obtained free of charge from The Cambridge Crystallographic Data Centre via www.ccdc.cam.ac.uk/data_request/cif.

Table 3. Crystal data and structure refinement for $[Mn(H_2O)(\mu\text{-}N_3)(N_3)(quinaz)_2]_n$ (**1**) and $[Mn(\mu\text{-}N_3)_2(quinaz)_2]_n$ (**2**).

Empirical formula	$C_{16}H_{14}MnN_{10}O$	$C_{16}H_{12}MnN_{10}$
Formula mass	417.31	399.30
Crystal system	triclinic	monoclinic
Space group	$P\bar{1}$	$C2/c$
a [Å]	7.6986(1)	18.4779(2)
b [Å]	10.9472(2)	6.8045(1)
c [Å]	11.7535(2)	12.8417(1)
α [°]	116.357(1)	90
β [°]	94.948(1)	99.920(1)
γ [°]	90.752(1)	90
V [Å^3]	882.81(2)	1590.48(3)
Z	2	4
T [K]	173(2)	173(2)
λ (Mo-K_α) [Å]	0.71073	0.71073
μ(Mo-K_α) [mm^{-1}]	0.780	0.857
$d_{calcd.}$ [g cm^{-3}]	1.570	1.668
Crystal size [mm]	$0.38 \times 0.20 \times 0.04$	$0.42 \times 0.36 \times 0.24$
Max./min. transmission	0.9695/0.7560	0.8207/0.7148
$\theta_{min./max.}$ [°]	1.94/32.87	2.24/32.95
Reflections collected	15595	13739
Independent refl./R_{int}	6160/0.0295	2876/0.0512
Parameters/observations	276/6160	132/2876
R [$I > 2\sigma(I)$][a]	0.0331	0.0373
R_w [all][b]	0.0861	0.0939

[a] $R(F_o) = \Sigma||F_o| - |F_c||/\Sigma|F_o|$. [b] $R_w(F_o)^2 = \{\Sigma w[(F_o)^2 - (F_c)^2]^2/[\Sigma w(F_o)^4]\}^{1/2}$.

Acknowledgments

This work was supported by the SIDA–Swedish Research Links program (grants 348-2002-6879 and 348-2004-5473) and the CICYT project PB03/0538.

[1] J. Ribas, A. Escuer, M. Monfort, R. Vicente, R. Cortés, L. Lezama, T. Rojo, *Coord. Chem. Rev.* **1999**, *193–195*, 1027.
[2] M. L. Hernández, M. G. Barandika, M. K. Urtiaga, R. Cortés, L. Lezama, M. I. Arriortua, *J. Chem. Soc., Dalton Trans.* **2000**, 79.
[3] M. A. M. Abu-Youssef, A. Escuer, D. Gatteschi, M. A. S. Goher, F. A. Mautner, R. Vicente, *Inorg. Chem.* **1999**, *38*, 5716.
[4] A. Escuer, R. Vicente, M. A. S. Goher, F. A. Mautner, *Inorg. Chem.* **1998**, *37*, 782.
[5] J. L. Manson, A. M. Arif, J. S. Miller, *Chem. Commun.* **1999**, 1479.
[6] J. Cano, Y. Journaux, M. A. S. Goher, M. A. M. Abu-Youssef, F. A. Mautner, G. J. Reib, A. Escuer, R. Vicente, *New J. Chem.* **2005**, *29*, 306.
[7] A. Escuer, F. A. Mautner, M. A. S. Goher, M. A. M. Abu-Youssef, R. Vicente, *Chem. Commun.* **2005**, 605.
[8] A. Escuer, R. Vicente, F. A. Mautner, M. A. S. Goher, M. A. M. Abu-Youssef, *Chem. Commun.* **2002**, 64.
[9] M. A. S. Goher, M. A. M. Abu-Youssef, F. A. Mautner, A. Escuer, R. Vicente, *Eur. J. Inorg. Chem.* **2000**, 1819.
[10] A. Escuer, C. J. Harding, Y. Dussart, J. Nelson, V. McKee, R. Vicente, *J. Chem. Soc., Dalton Trans.* **1999**, 223.
[11] M. E. Fisher, *Am. J. Phys.* **1964**, *32*, 343.
[12] R. Cortés, M. Drillon, X. Solans, L. Lezama, T. Rojo, *Inorg. Chem.* **1997**, *36*, 677.
[13] M. E. Lines, *J. Phys. Chem. Solids* **1970**, *31*, 101.
[14] A. Escuer, R. Vicente, M. A. S. Goher, F. A. Mautner, *Inorg. Chem.* **1998**, *37*, 782.
[15] *SMART & SAINT, Area Detector Control and Integration Software*, Siemens AXS, Madison, WI, USA, **1995**.
[16] G. M. Sheldrick, *SADABS, Program for Empirical Absorption Correction of Area Detectors*, version 2.03, University of Göttingen, Germany, **2002**.
[17] *SHELXTL, Structure Determination Programs*, version 6.10, Bruker AXS Inc., Madison, Wisconsin, USA, **2001**.
[18] K. Brandenburg, *Diamond, Visual Crystal Structure Information System*, version 2.1e, Crystal Impact GbR, Bonn, Germany, **2001**.

Received: April 22, 2005
Published Online: October 5, 2005

